**Supplemental Information for:**
***Material microenvironmental properties couple to induce distinct transcriptional programs in mammalian stem cells***

Contents:



## Methods

### Casting of Alginate Hydrogels

Alginate type LF20/40 (FMC Biopolymer) was used as-received for the slow-relaxing hydrogels and was irradiated with an 8mRad cobalt source to form the fast-relaxing hydrogels. Alginates were modified with GGGGRGDSP peptides (Peptide 2.0) at the reported densities with standard carbodiimide chemistry as described previously(1). After modification, alginates were dialyzed against a NaCl gradient, treated with activated charcoal, and sterile-filtered. After lyophilization, all alginate was dissolved in serum-free DMEM (Lonza) at 2.5%.

Hydrogels were cast by rapidly mixing the alginate solution with a $CaSO_4$ slurry via two syringes and ejecting the mixture between two glass plates, where it gelled over 1.5 hours.

For mMSC culture experiments, stiff slow-relaxing gels consisted of 2% LF20/40 alginate and 82mM Ca, while stiff fast relaxing gels consisted of 2% LF20/40 8mRad alginate (referring to the lower molecular weight, irradiated alginate) and 199mM Ca. Intermediate stiffness slow-relaxing gels consisted of 2% LF20/40 alginate and 20mM

Ca, while intermediate stiffness fast relaxing gels consisted of 2% LF20/40 8mRad alginate and 42mM Ca. Soft slow-relaxing gels consisted of 2% LF20/40 alginate and 8mM Ca, while fast relaxing gels consisted of 2% LF20/40 8mRad alginate and 19mM Ca. This difference in calcium concentration has previously been noted to have no effect on mesenchymal stem cell viability and differentiation(2, 3). 8mm disks were then cut from the gel using a biopsy punch.

For hNPC culture experiments, stiff slow-relaxing gels consisted of 2% LF20/40 alginate and 16mM Ca, while stiff fast relaxing gels consisted of 2% LF20/40 8mRad alginate and 34mM Ca. Soft slow-relaxing gels consisted of 2% LF20/40 alginate and 5mM Ca, while soft fast relaxing gels consisted of 2% LF20/40 8mRad alginate and 13mM Ca. 8mm disks were then cut from the gel using a biopsy punch.

**Adhesion Ligand Density (RGD Peptide) Quantification**

RGD coupling density was determined using the LavaPep assay following the manufacturers instructions. Coupled alginate was dissolved at a concentration of 0.1 mg/mL in PBS before incubation with the LavaPep reagents. A standard curve of GGGGRGDSP peptides was prepared in PBS containing 0.1 mg/mL uncoupled alginate as background. Fluorescence was read using a Biotek plate reader and the resulting concentration was used to find the molar ratio of alginate to peptide. Molar concentration of peptide was calculated assuming a 2% alginate gel from the molar ratio. Reported values are consistent with previous studies using identical protocols (2).

**Justification for Physiologic Range of Adhesion Ligand Concentration**

Two methods were used to derive relevant physiologic ranges of adhesion ligand concentration. Developing de-cellularized myocardium was found by mass spectroscopy to contain predominantly Collagen I at a concentration of ~500ng collagen/g tissue(4). At a 2% protein concentration, comparable to our hydrogel's overall polymer content, this implies a 1e15 collagens/mL. With seven integrin binding sites per collagen, this value implies a 70 μM concentration of integrin binding sites.

A second reference measured collagen concentrations in breast tissue, finding ~50mg/mL collagen(5). At a molecular weight of ~300kDa, this concentration is equivalent to 170 μM. Again, at seven integrin binding sites per collagen, this value implies a binding site concentration of 1190 μM.

Additionally, Fischbach et al. reported and adhesion ligand concentration of 142 μM in tumor-associated matrix(6).

Hence, given these methods to estimate an order of magnitude for the number of adhesion sites, and given numerous other papers that show at least tenfold changes in ECM component concentrations as a function of tissue, age, and disease, our range of adhesion ligand densities falls within a physiologically reasonable range.

**Hydrogel Mechanical Characterization**

Hydrogels were fabricated as described above at a thickness of 2mm and subjected to compression testing using a mechanical testing device (Instron). Gels were compressed at a strain rate of 1mm/min and the Young's Modulus was calculated as the best-fit slope of the first 5-15% of the resulting stress/strain curve. At 15% strain, the strain was held and the time required for the stress to decay by a factor of two was noted.

15% strain was chosen based on previous reports of cell-mediated strains in hydrogels and tissues. Material strains of 20-30% have been observed in the vicinity of fibroblasts in 3D hydrogel culture(7), while strains of 40% have been reported in the skin of the knee(8), 30% in muscles during contraction(9), and around 15% in the lung during breathing(10), suggesting that materials experience comparable levels of strain in cell-laden environments.

**mMSC Cell Culture**

D1 mouse mesenchymal stem cells (MSCs) (ATCC) were encapsulated in the hydrogels during the mixing step at a concentration of 10 million cells/mL. Immediately before mixing, cells were rinsed and centrifuged twice to ensure the removal of any residual ECM components. After casting and punching, gels were placed in 24-well plates and cultured at 37 C in DMEM (Lonza) with 10% fetal bovine serum and 1% penicillin/streptomycin.

In order to confirm that the mMSCs used were functionally similar to those used in previous studies, we cultured mMSCs until the 40 hour time point in slow-relaxing, high ligand density 3kPa and 18kPa alginate hydrogels without differentiation supplements

and stained the cells for markers of adipogenic differentiation (lipid droplets, Oil Red O) and osteogenic differentiation (alkaline phosphatase, Fast Blue) (Fig. S4). We observed no staining for adipogenic differentiation and a slightly positive Fast Blue stain in the 18kPa case, consistent with previous studies (3) and confirming the expected uncommitted nature of the MSCs and their differentiation potential.

**Live-Dead Staining**

Gels were treated with Life Technologies Live/Dead reagent per the manufacturer's specifications and were then transferred to a microscope slide with a custom-made PDMS well. A coverslip was placed over the hydrated gel and the gels were imaged on a Zeiss LSM 710 upright confocal microscope. Viability was quantified by computing the number of live and dead cells across five representative fields of view using ImageJ.

**MSC Differentiation Staining**

After 40 hours of culture, gels were removed from wells and washed twice with PBS containing calcium and magnesium (PBS++, Gibco) before fixation with 4% paraformaldehyde in PBS++ for 45 minutes on an orbital shaker. Gels were then washed and transferred into a 30% sucrose in PBS++ solution overnight at 4C. This solution was then diluted 1:1 with optimal cutting temperature compound (OCT) and gels were again soaked overnight. A final overnight incubation in 100% OCT was performed before freezing the gels on dry ice and storage at -80C. Cryosectioning was performed at a thickness of 30 microns and sections were dried at room temperature before staining.

Prior to each staining protocol, OCT was removed from the sections by washing twice with PBS++ for 5 minutes each wash.

For fast blue staining, sections were incubated for 15 min. in alkaline buffer (100mM Tris-HCl, 100mM NaCl, 0.1% Tween-20, 50mM MgCl2, pH 8.2). Sections were then incubated in a staining solution of: 500 μg/ml naphthol-AS- MX phosphate, 500 μg/ml Fast Blue BB salt in alkaline buffer for 45 minutes at room temperature. Sections were washed in alkaline buffer then PBS++ before imaging.

For oil red O staining, sections were equilibrated in 60% isopropanol for 5 minutes before staining with 1.8mg/mL oil red O in 60% isopropanol for 10 minutes. Sections were washed with PBS++ before imaging.

**Cell Retrieval from Gels**

After 40 hours of culture, gels were removed from the wells and placed into eppendorf tubes with 50mM EDTA in HEPES on ice for 10 minutes. An equal volume of trypsin-EDTA was then added to the tubes for an additional 5 minutes at 37C to ensure the removal of cells from the alginate chains. Cells were centrifuged and rinsed twice before proceeding to additional analysis.

**Cell Counting for Proliferation Analysis**

After cell retrieval as described above, cells were diluted per the manufacturer's instructions and counted on a Countess FLII automated cell counter (Life Technologies). Cell counts were compared to the original encapsulated cell numbers.

**RNA-seq**

After cell retrieval as described above, cells were lysed and total RNA was extracted per manufacturer's instructions with the Qiagen RNeasy Micro kit. Samples were then submitted to the Harvard Medical School Biopolymers Facility, where mRNA enrichment and library preparation was performed. Individual samples were barcoded and run on either an Illumina HiSeq 2500 Rapid or an Illumina NextSeq. The data presented here represents two independent sequencing experiments that were pooled to yield the reported number of replicates per sample. Data will be deposited in the relevant databases before publication.

**Statistical Methods**

Statistics for RNA-seq experiments are described in the RNA-seq Analysis section. For flow cytometry for the mMSC immunomodulation and MSC/HSPC crosstalk experiments, Igor Pro software was used to run one-way ANOVA, followed by a Tukey-post-hoc test.

**mMSC RNA-seq Differential Expression Analysis**

Raw reads were aligned to the UCSC Genome Browser mm10 genome using Subread(11) and counts were aggregated per gene using FeatureCounts(12). After

aggregating read counts, we performed TMM normalization. Voom(13) and Limma(14) were then used to perform differential expression analysis using a multi-level factorial design. Batch was accounted for with an additional factor in the linear model. Differentially-expressed genes were defined as those with a fold-change of at least 2 and a BH-adjusted p-value of less than 0.05. For visualization and clustering, Combat was used to remove batch effects. TPM used for visualization and clustering was calculated after applying TMM normalization and variance stabilization to the Combat cleaned counts. Principal component analysis was coded manually using the log-transformed TPM for each biological replicate. qPCR on selected transcripts and material conditions mirrored the sequencing results (Fig. S16). Code used to run analysis is available upon request.

For Fig. 1 B,F, the number of DE genes for the reported comparisons was taken from the non-interaction terms of the linear model. We refer to these sets of genes as the "decoupled" genes.

For Fig. 1C,G, the number of DE genes for each comparison between conditions was found and plotted as a circle, with the area corresponding to the number of DE genes. For Fig. 1D,H, the intersection of the DE genes from each comparison and from the decoupled Venn Diagram were identified. Each intersection then represented a slice of the pie chart that represented all DE genes for that comparison. The resulting pie charts were plotted color-coded to the decoupled Venn Diagram gene sets.

**Neural Progenitor Production**

The human iPSC line 1016a (certified mycoplasma negative and karyotypically normal) was differentiated using a published cortical neuron protocol. Briefly, iPSC cells were dissociated to single cells and seeded into a spinning bioreactor at a concentration of $1x10^6$ cells/mL in mTesr media (Stem Cell Technologies) supplemented with Rock inhibitor (10µM). On day 2, dual SMAD (SB431542, 10µM; LDN193189, 100nM) and Wnt inhibition (XAV939, 2µM) were used to pattern the iPSC to a neural fate. From day 3 to 10, the culture was transitioned from 100% KSR media (15% Knock Out Serum Replacement, KnockOut DMEM, 1x Glutamax, 1x NEAA, 1x Pen/Strep, 1x BME) to 100% NIM media (DMEM-F12,1x N2 supplement, 1x B27 -VitA Supplement, 1x Glutamax, 1x NEAA, 1x Pen/Strep). On day 10, the spheres were collected, washed in DPBS, and dissociated with 0.05% Trypsin. Once dissociated, cells were passed through a 70µm filter, counted with Trypan Blue, and plated at 50,000 cells per well. Cells were plated on a Greiner microclear 96 well plate coated with laminin, polyornithine, and fibronectin.

24 hours after plating, cells were fixed with 4% paraformaldehyde, permeabilized 0.1% Triton and blocked with 1% BSA, 5% FBS in DPBS. Primary antibodies were then added in blocking solution overnight at 4°C at the following concentrations: rbαPax6 1:600 (Biolegend cat# 901301), msαSOX2 1:200 (Cell Signaling Technology cat# 4900S). The next day, cells were washed and secondary antibodies, gtαrb Alexa 546 and gtαms Alexa 488, were used at 1:1000 and Hoechst nuclear stain was added at 1:5000 in DPBS. The stained plate was imaged on a Perkin Elmer Phenix with a 20x water objective. 30

wells, 20 fields each, were analyzed using the Columbus software package (Perkin Elmer). The percentage of SOX2+/Pax6+ cells were calculated by comparison with the total nuclei counted via Hoechst staining. 75% of cells were found to be Pax6+ and 60% were found to be SOX2+/Pax6+ (Fig. S8,9).

**hNPC Cell Culture**

After production, hNPCs were encapsulated in the hydrogels during the mixing step at a concentration of 5 million cells/mL. Immediately before mixing, cells were rinsed and centrifuged twice to ensure the removal of any residual ECM components. After casting and punching, gels were placed in 24-well plates and cultured at 37 C in NIM media (described above). Cells were stained for viability as described for mMSCs and were found to be highly viable and evenly distributed throughout the gel (Fig. S9).

**hNPC RNA-seq Differential Expression Analysis**

Raw reads were aligned to the UCSC Genome Browser hg38 genome using Subread(11) and counts were aggregated per gene using FeatureCounts(12). After aggregating read counts, we performed TMM normalization. Voom(13) and Limma(14) were then used to perform differential expression analysis using a multi-level factorial design. Differentially-expressed genes were defined as those with a fold-change of at least 4 and a BH-adjusted p-value of less than 0.05. TPM used for visualization and clustering was calculated after applying TMM normalization and variance stabilization. Principal component analysis was coded manually using the log-transformed TPM for each biological replicate.

**Weighted Gene Coexpression Network Analysis (WGCNA)**

WGCNA(15) was run on the Combat-cleaned TPM data and the topological overlap matrix was calculated using an unsigned network and a soft power of 10. Modules were defined using the dynamic tree cut algorithm. Module significance for stiffness, stress relaxation, and ligand density was computed for each module by correlating the expression of module member genes each parameter encoded as low (0) or high (1) and taking the average gene significance for that module. The most significant genes for each module were found using the NetworkScreening function and were defined as those having high module membership and high intra-modular connectivity. For the hNPCs, a soft power of 20 was used.

**Metacore Network Analysis and Visualization**

For Figure 3, the member genes for the three modules of interest were used as the seed genes to identify inferred PathwayMaps (Fig. 3b). In Fig. 3c, the member genes from the three modules of interest were combined and used as seeds for the Metacore AnalyzeNetwork function. This function yields sub-networks that are ranked by an enrichment score. We selected and merged the top three sub-networks to arrive at the network shown in Fig. 3c, which represents a putative version of a network that captures material-sensing behaviors across our parameters of interest. In Fig. 3d, the member genes corresponding to modules with high or low module-module correlations were used

as seeds and the PathwayMap enrichment analysis was performed. P-values are BH-adjusted.

For the drug target analysis, DE genes for hNPCs corresponding to stress relaxation, stiffness, and ligand density were pooled and fed into the Drug Target pipeline in Metacore. The drug hits in the "therapeutic drug-target interactions" list were taken.

**qPCR**

Cells were retrieved from gels as described above and total RNA was extracted using the Qiagen RNeasy micro kit following manufacturer's instructions. Reverse transcription was carried out using BioRad iScript Advanced cDNA synthesis kit and PrimePCR validated primers (Table S1) along with BioRad sso Advanced Universal SYBR Green Supermix were used for the qPCR assay. Samples were run on a BioRad QFX96 at the Harvard Center for Systems Biology Bauer Core facility. Relative expression was calculated from normalized ΔCt values using a GAPDH housekeeping gene.

**MSC-HSPC Coculture Experiment**

HSPCs were isolated from the tibia, femur, and pelvis of 6-12 week old wild type C57BL/6 mice. Isolated bones were abraded to remove muscle tissue, crushed in a mortar and pestle, and strained through a 70 um mesh filter. Lin- ckit+ sca1+ (LKS) cells were isolated by first staining for these markers (Pacific Blue anti-mouse lineage cocktail CAT: 133310, PE anti-mouse Ly-6A/E (Sca-1) CAT: 108108, APC anti-mouse CD117

(c-kit) CAT: 105812) and then sorting using a 5-laser FACS Aria (Fig. S19). Alginate hydrogels were fabricated as indicated above at a thickness of 0.5mm and placed at the bottom of a well of a 12 well plate coated with pluronic in order to prevent rogue cell adhesion. A Transwell membrane was placed in each well and mouse HSPCs were seeded on the membrane. D1s were cocultured with hematopoietic cells in StemSpan SFEM (StemCell Technologies) supplemented with 10% FBS; 1% penicillin/streptomycin; and 10 ng/mL recombinant mouse SCF, FLT3L, and interleukin-7 (BioLegend). Media change was performed every two days, and the coculture was terminated after one week. Analytic flow cytometry was performed using a four-laser LSR II with diva software (Becton Dickinson). Cells were stained for the above antibodies as well as calcein-AM (Invitrogen) and CD45 (PE/Cy7 anti-mouse CD45 CAT: 103113). Analysis was performed using FlowJo 8.7 software.

**Conditioned Media Experiment**

Alginate hydrogels containing mMSCs were fabricated as indicated above for the coculture experiment, but without the Transwell insert and HSPCs. For two days, cells were cultured in DMEM (Lonza) with 10% fetal bovine serum and 1% penicillin/streptomycin, after which they were washed 3 times with PBS to remove residual serum and subsequently cultured in serum-free DMEM with 1% penicillin/streptomycin for one day. The media was collected after 24 hours and concentrated using a centrifugal filter (Pall). This conditioned media was used per the manufacturer's specifications in Abcam's ab193659 mouse 96-target cytokine array and chemiluminescence was read on a FluorChem M imager. Spot sizes for each cytokine

were measured using ImageJ and sizes were averaged over duplicates included on each array.

To check the general correspondence between the RNA-seq data and the cytokine array, we calculated average expression for the fifteen cytokines common to both the array and the RNA-seq dataset. Of those, we found six to qualify as differentially expressed. Since the difference in sensitivity between the array and RNA-seq data does not allow for a direct comparison, we sought to verify the general trends by asking, within this set of DE cytokines, for how many of the cytokines was the highest expression condition consistent between the array and RNA-seq. We found that in five of six cytokines, the highest conditioned matched (Fig. S 18).

**Supplemental Figures**

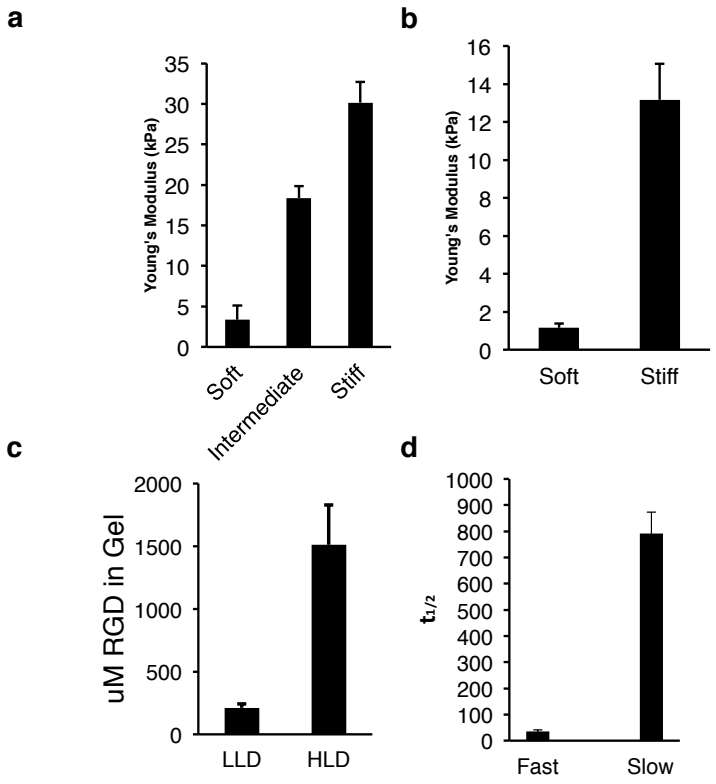


317
318 **Figure S1:** Characterization of RGD-coupled alginate hydrogels

319 a) Young's Moduli of alginate hydrogels used for mMSC culture. Mean + S.D.

320 b) Young's Moduli of alginate hydrogels used for hNPC culture. Mean + S.D.

321 c) Quantification of RGD coupling per LavaPep assay. Mean + S.D.

322 d) Time to achieve 50% relaxation of maximal stress in hydrogels when held at 15%

323 strain. Mean + S.D.

324

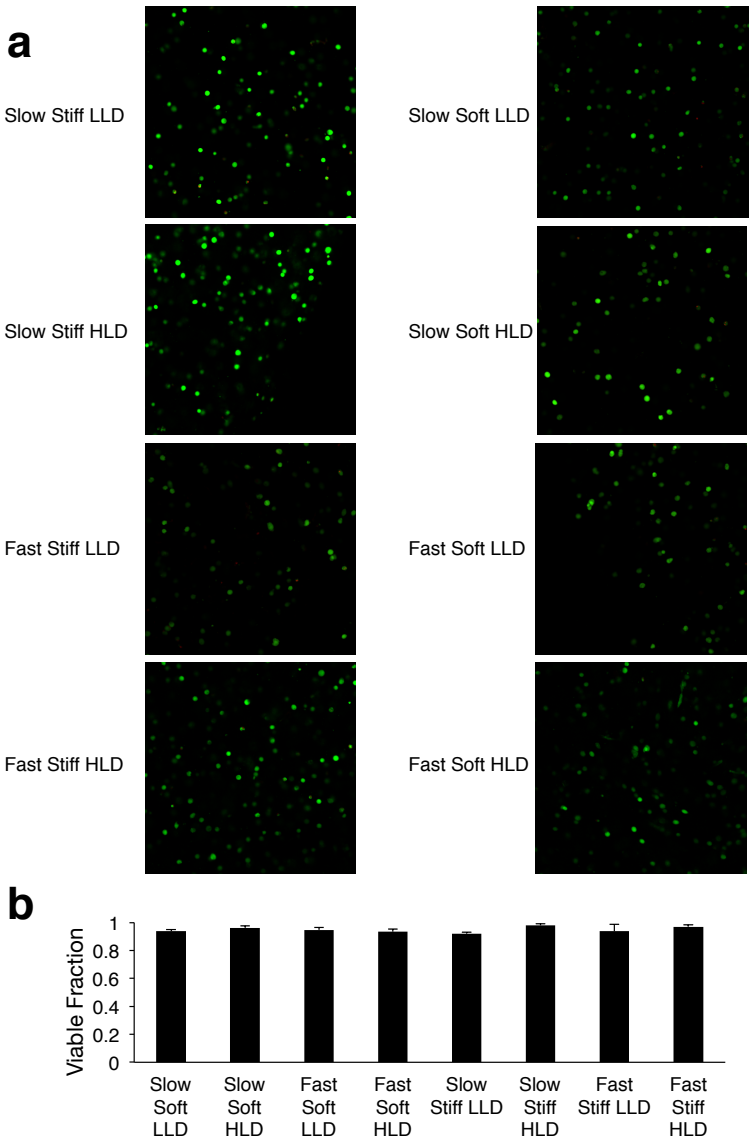


**Figure S2:** Viability and distribution of MSCs in hydrogels

a) Live/Dead staining of MSCs in hydrogels. Live cells appear green and dead cells appear red.

b) Quantification of fraction of viable cells in hydrogels, computed from five representative fields of view for each gel. Cells were segmented and counted using ImageJ. Mean + S.D.

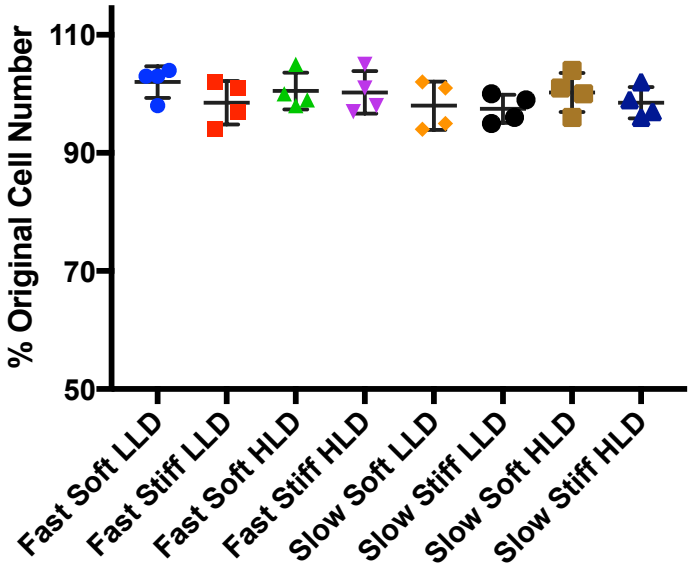


**Figure S3**: Percentage of original mMSC cell numbers after 2 days in culture in alginate hydrogels. No statistical significance found with ANOVA. Error bars, S.D.

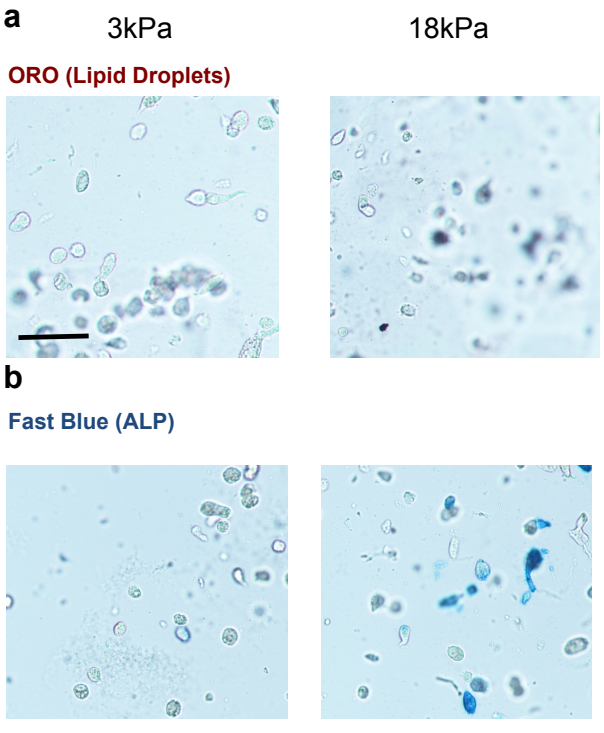

**Figure S4:** Differentiation staining of mMSCs at 40 hours. A) Oil Red O staining for lipid droplets in mMSCs in sections of soft and stiff, high ligand density, slow-relaxing hydrogels. Scale bar - 60μm. B) A) Fast Blue staining for alkaline phosphatase in mMSCs in sections of soft and stiff, high ligand density, slow-relaxing hydrogels. Scale bar - 60μm.

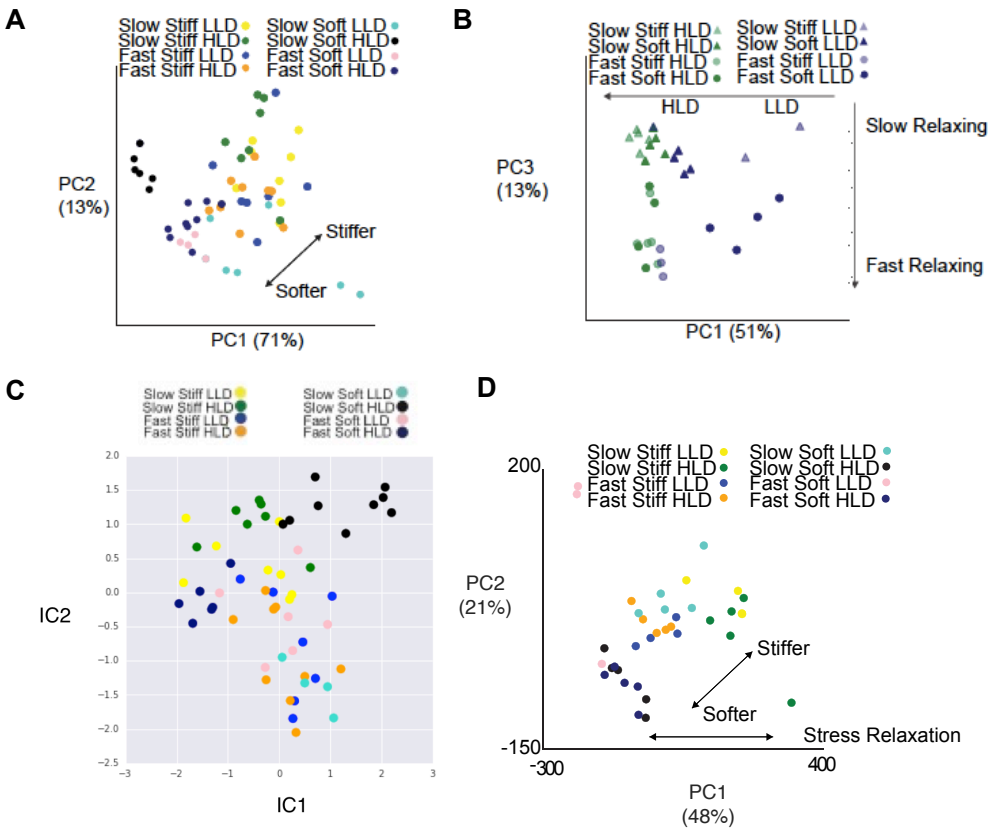


**Figure S5: Clustering analysis of MSC RNA-seq data**

a) Principal component analysis of gene expression in mMSCs across all replicates for each material with 30kPa as the stiff material. PC1, first principal component, etc. Light purple triangle, Slow Stiff Low Ligand Density. Light green triangle, Slow Stiff High Ligand Density. Light purple circle, Fast Stiff Low Ligand Density. Light green circle, Fast Stiff High Ligand Density. Dark purple triangle, Slow Soft Low Ligand Density. Dark green triangle, Slow Soft High Ligand Density. Dark purple circle, Fast Soft Low Ligand Density. Dark green circle, Fast Soft High Ligand Density. Each point represents a sequencing replicate. Arrows represent directions along which the variation for that specific substrate property is captured.

b) Principal component analysis of gene expression in mMSCs across all replicates for each material with 18kPa as the stiff material. Yellow, Slow Stiff Low Ligand Density. Green, Slow Stiff High Ligand Density. Purple, Fast Stiff Low Ligand Density. Orange, Fast Stiff High Ligand Density. Turquoise, Slow Soft Low Ligand Density. Black, Slow Soft High Ligand Density. Pink, Fast Soft Low Ligand Density. Navy, Fast Soft High Ligand Density. Each point represents a sequencing replicate. Arrows represent directions along which the variation for that specific substrate property is captured.

c) Independent component analysis of gene expression in mMSCs across all replicates for each material. IC1 represents the first independent component and IC2 represents the second independent component. Yellow, Slow Stiff Low Ligand Density. Green, Slow Stiff High Ligand Density. Purple, Fast Stiff Low Ligand Density. Orange, Fast Stiff High Ligand Density. Turquoise, Slow Soft Low Ligand Density. Black, Slow Soft High Ligand Density. Pink, Fast Soft Low Ligand Density. Navy, Fast Soft High Ligand Density. Each point represents a sequencing replicate.

d) Principal component analysis of gene expression in hNPCs across all replicates for each material. PC1, first principal component, etc. Yellow, Slow Stiff Low Ligand Density. Green, Slow Stiff High Ligand Density. Purple, Fast Stiff Low Ligand Density. Orange, Fast Stiff High Ligand Density. Turquoise, Slow Soft Low Ligand Density. Black, Slow Soft High Ligand Density. Pink, Fast Soft Low Ligand Density. Navy, Fast Soft High Ligand Density. Each point represents a

sequencing replicate. Arrows represent directions along which the variation for that specific substrate property is captured.

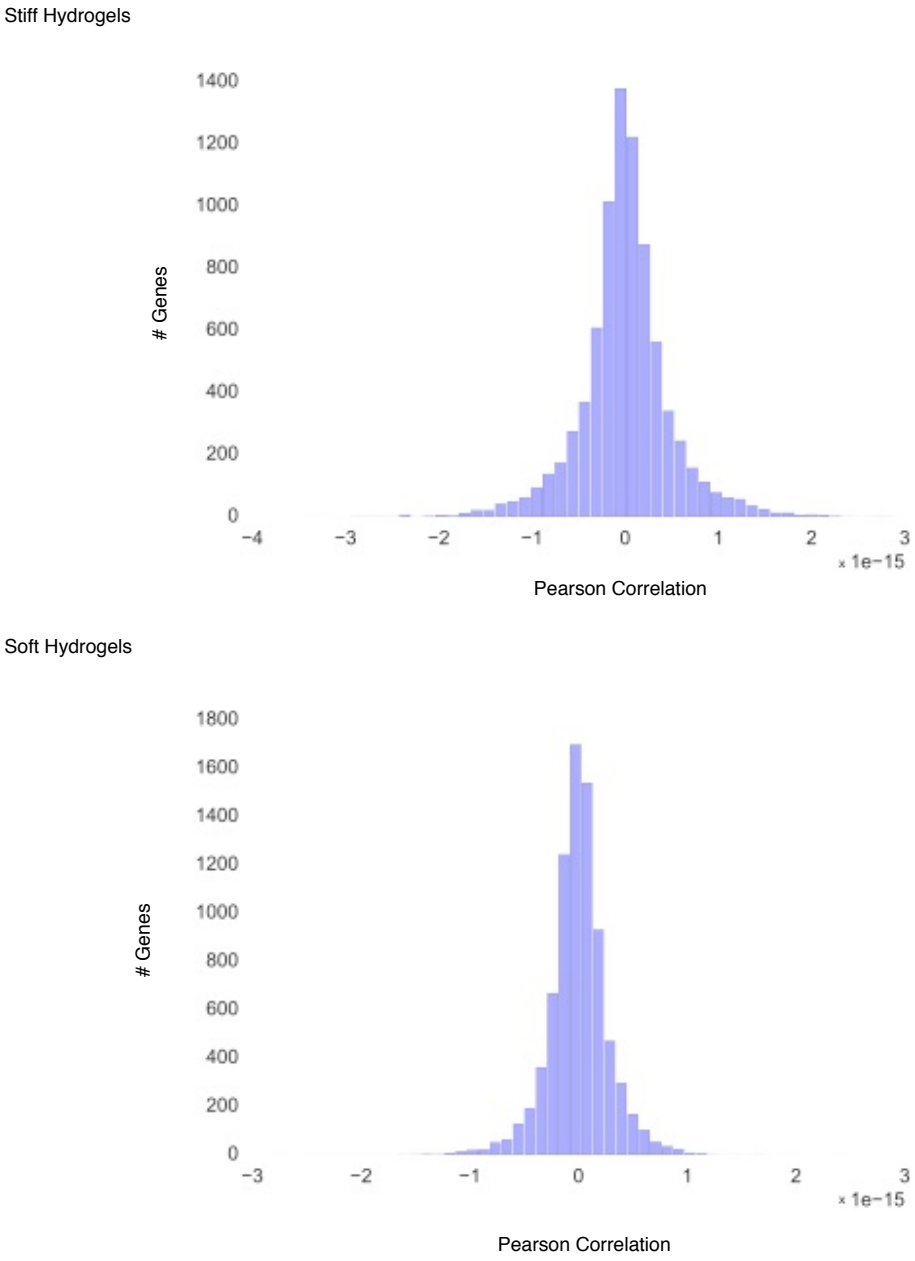


**Fig. S6:** Distributions across all genes in mMSCs of Pearson correlations of gene expression as a function of hydrogel Ca concentration for soft and stiff hydrogels. All replicates were used to calculate the correlations.

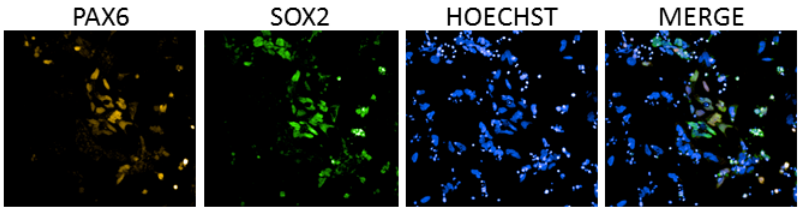


**Figure S7:** Characterization of hNPC markers. Representative images of staining for Pax6 and Sox2 24 hours after retrival from spheroid culture, and thus representative of the cell state prior to encapsulation in hydrogels.

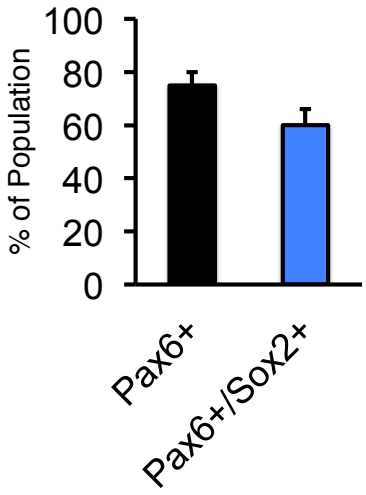


**Figure S8:** Quantification of hNPC markers in population. Quantification from epresentative images of staining for Pax6 and Sox2 24 hours after retrieval from spheroid culture, and thus representative of the cell state prior to encapsulation in hydrogels. Mean +/- S.D

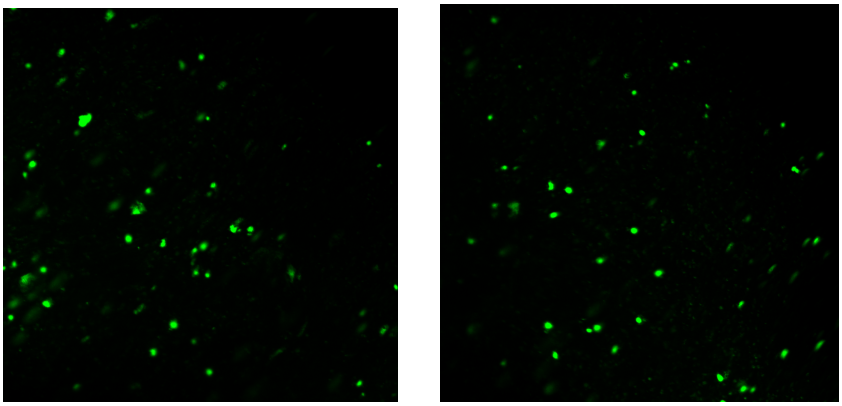


**Figure S9:** Viability and distribution of hNPCs encapsulated in hydrogels two days post encapsulation. Representative confocal images show live cells staining green and dead cells staining red, along with the distribution of mostly single cells.

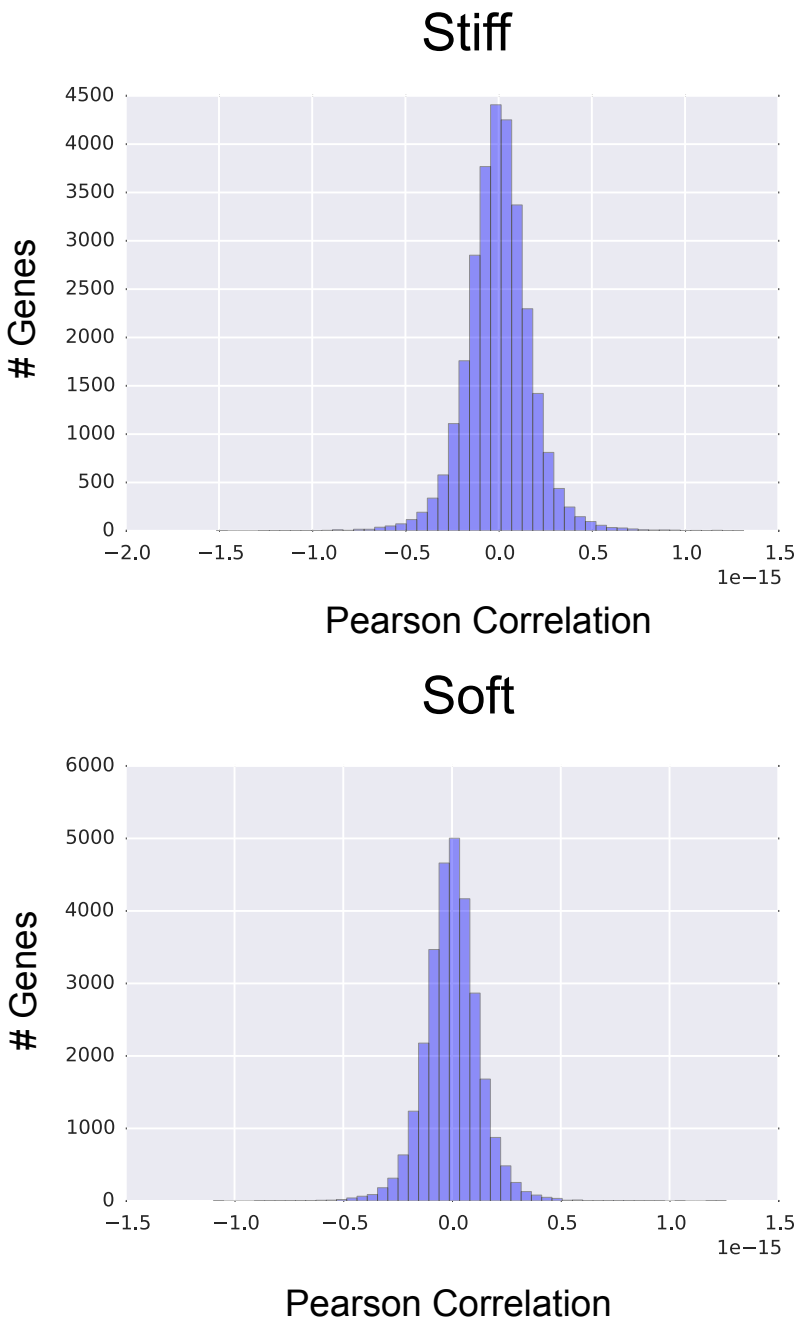


404

405 **Fig. S10:** Distributions across all genes in hNPCs of Pearson correlations of gene

406 expression as a function of hydrogel Ca concentration for soft and stiff hydrogels. All

407 replicates were used to calculate the correlations.

408

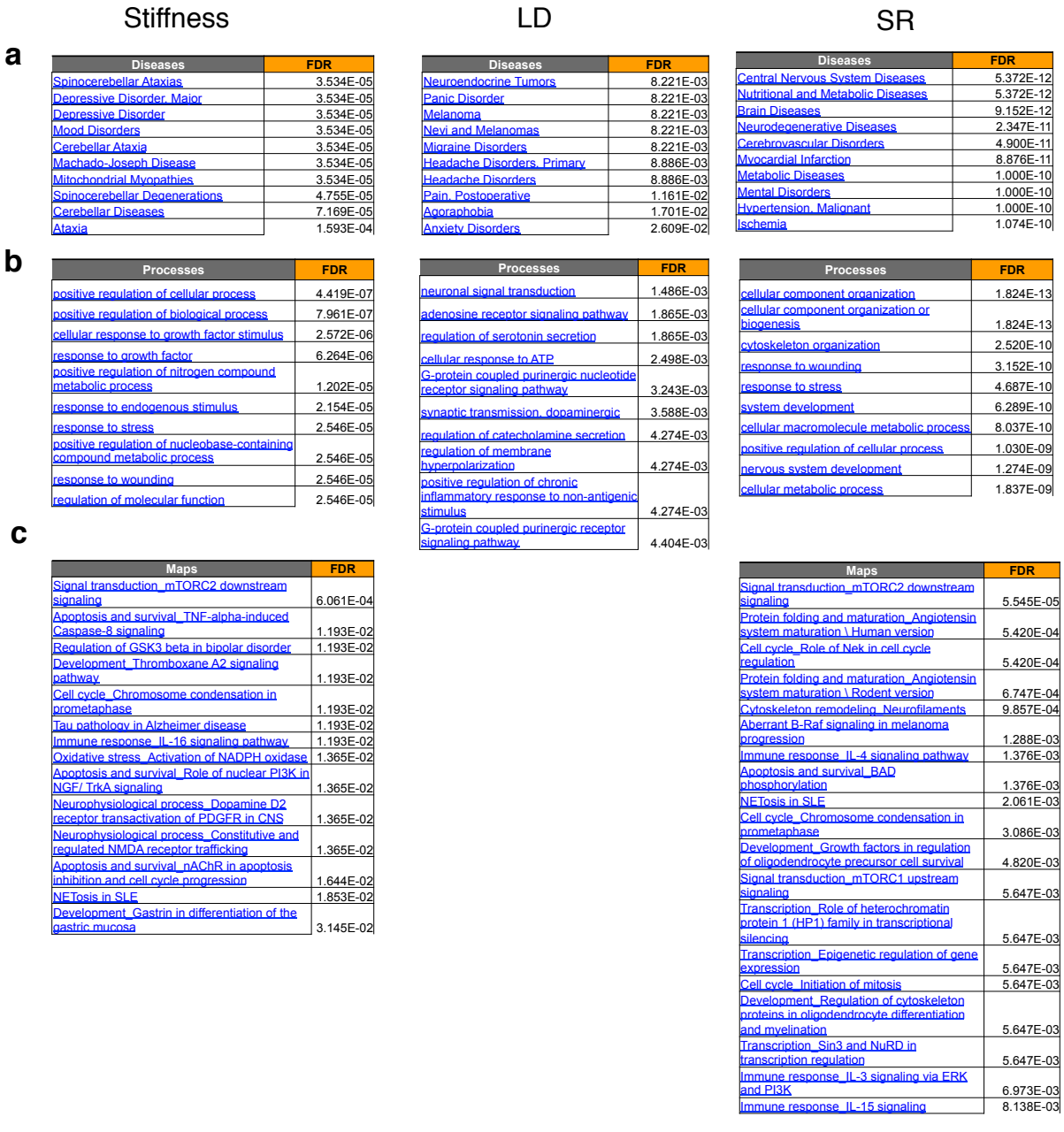


**a**

| Stiffness: Diseases | FDR |
|---|---|
| Spinocerebellar Ataxias | 3.534E-05 |
| Depressive Disorder, Major | 3.534E-05 |
| Depressive Disorder | 3.534E-05 |
| Mood Disorders | 3.534E-05 |
| Cerebellar Ataxia | 3.534E-05 |
| Machado-Joseph Disease | 3.534E-05 |
| Mitochondrial Myopathies | 3.534E-05 |
| Spinocerebellar Degenerations | 4.755E-05 |
| Cerebellar Diseases | 7.169E-05 |
| Ataxia | 1.593E-04 |

| LD: Diseases | FDR |
|---|---|
| Neuroendocrine Tumors | 8.221E-03 |
| Panic Disorder | 8.221E-03 |
| Melanoma | 8.221E-03 |
| Nevi and Melanomas | 8.221E-03 |
| Migraine Disorders | 8.221E-03 |
| Headache Disorders, Primary | 8.886E-03 |
| Headache Disorders | 8.886E-03 |
| Pain, Postoperative | 1.161E-02 |
| Agoraphobia | 1.701E-02 |
| Anxiety Disorders | 2.609E-02 |

| SR: Diseases | FDR |
|---|---|
| Central Nervous System Diseases | 5.372E-12 |
| Nutritional and Metabolic Diseases | 5.372E-12 |
| Brain Diseases | 9.152E-12 |
| Neurodegenerative Diseases | 2.347E-11 |
| Cerebrovascular Disorders | 4.900E-11 |
| Myocardial Infarction | 8.876E-11 |
| Metabolic Diseases | 1.000E-10 |
| Mental Disorders | 1.000E-10 |
| Hypertension, Malignant | 1.000E-10 |
| Ischemia | 1.074E-10 |

**b**

| Stiffness: Processes | FDR |
|---|---|
| positive regulation of cellular process | 4.419E-07 |
| positive regulation of biological process | 7.961E-07 |
| cellular response to growth factor stimulus | 2.572E-06 |
| response to growth factor | 6.264E-06 |
| positive regulation of nitrogen compound metabolic process | 1.202E-05 |
| response to endogenous stimulus | 2.154E-05 |
| response to stress | 2.546E-05 |
| positive regulation of nucleobase-containing compound metabolic process | 2.546E-05 |
| response to wounding | 2.546E-05 |
| regulation of molecular function | 2.546E-05 |

| LD: Processes | FDR |
|---|---|
| neuronal signal transduction | 1.486E-03 |
| adenosine receptor signaling pathway | 1.865E-03 |
| regulation of serotonin secretion | 1.865E-03 |
| cellular response to ATP | 2.498E-03 |
| G-protein coupled purinergic nucleotide receptor signaling pathway | 3.243E-03 |
| synaptic transmission, dopaminergic | 3.588E-03 |
| regulation of catecholamine secretion | 4.274E-03 |
| regulation of membrane hyperpolarization | 4.274E-03 |
| positive regulation of chronic inflammatory response to non-antigenic stimulus | 4.274E-03 |
| G-protein coupled purinergic receptor signaling pathway | 4.404E-03 |

| SR: Processes | FDR |
|---|---|
| cellular component organization | 1.824E-13 |
| cellular component organization or biogenesis | 1.824E-13 |
| cytoskeleton organization | 2.520E-10 |
| response to wounding | 3.152E-10 |
| response to stress | 4.687E-10 |
| system development | 6.289E-10 |
| cellular macromolecule metabolic process | 8.037E-10 |
| positive regulation of cellular process | 1.030E-09 |
| nervous system development | 1.274E-09 |
| cellular metabolic process | 1.837E-09 |

**c**

| Stiffness: Maps | FDR |
|---|---|
| Signal transduction_mTORC2 downstream signaling | 6.061E-04 |
| Apoptosis and survival_TNF-alpha-induced Caspase-8 signaling | 1.193E-02 |
| Regulation of GSK3 beta in bipolar disorder | 1.193E-02 |
| Development_Thromboxane A2 signaling pathway | 1.193E-02 |
| Cell cycle_Chromosome condensation in prometaphase | 1.193E-02 |
| Tau pathology in Alzheimer disease | 1.193E-02 |
| Immune response_IL-16 signaling pathway | 1.193E-02 |
| Oxidative stress_Activation of NADPH oxidase | 1.365E-02 |
| Apoptosis and survival_Role of nuclear PI3K in NGF/ TrkA signaling | 1.365E-02 |
| Neurophysiological process_Dopamine D2 receptor transactivation of PDGFR in CNS | 1.365E-02 |
| Neurophysiological process_Constitutive and regulated NMDA receptor trafficking | 1.365E-02 |
| Apoptosis and survival_nAChR in apoptosis inhibition and cell cycle progression | 1.644E-02 |
| NETosis in SLE | 1.853E-02 |
| Development_Gastrin in differentiation of the gastric mucosa | 3.145E-02 |

| SR: Maps | FDR |
|---|---|
| Signal transduction_mTORC2 downstream signaling | 5.545E-05 |
| Protein folding and maturation_Angiotensin system maturation \ Human version | 5.420E-04 |
| Cell cycle_Role of Nek in cell cycle regulation | 5.420E-04 |
| Protein folding and maturation_Angiotensin system maturation \ Rodent version | 6.747E-04 |
| Cytoskeleton remodeling_Neurofilaments | 9.857E-04 |
| Aberrant B-Raf signaling in melanoma progression | 1.288E-03 |
| Immune response_IL-4 signaling pathway | 1.376E-03 |
| Apoptosis and survival_BAD phosphorylation | 1.376E-03 |
| NETosis in SLE | 2.061E-03 |
| Cell cycle_Chromosome condensation in prometaphase | 3.086E-03 |
| Development_Growth factors in regulation of oligodendrocyte precursor cell survival | 4.820E-03 |
| Signal transduction_mTORC1 upstream signaling | 5.647E-03 |
| Transcription_Role of heterochromatin protein 1 (HP1) family in transcriptional silencing | 5.647E-03 |
| Transcription_Epigenetic regulation of gene expression | 5.647E-03 |
| Cell cycle_Initiation of mitosis | 5.647E-03 |
| Development_Regulation of cytoskeleton proteins in oligodendrocyte differentiation and myelination | 5.647E-03 |
| Transcription_Sin3 and NuRD in transcription regulation | 5.647E-03 |
| Immune response_IL-3 signaling via ERK and PI3K | 6.973E-03 |
| Immune response_IL-15 signaling | 8.138E-03 |

**Figure S11:** Enrichment analysis of hNPC DE genes.
a) Top 10 diseases significantly enriched in the DE genes for each of the material parameters of interest.
b) Top gene ontology processes significantly enriched in the DE genes for each of the material parameters of interest.
c) Top Metacore Pathway Maps significantly enriched in the DE genes for stiffness and stress relaxation. Statistics account for multiple hypotheses and were calculated automatically with Metacore's enrichment function.

| Drug | Target |
|---|---|
| Acetazolamide intracellular | CA3 |
| Carbonic anhydrase XI | CA11 |
| Ridaforolimus intracellular | MTOR |
| Docetaxel intracellular | TUBB |
| Bupivacaine extracellular region | KCNA5 |
| Riviciclib intracellular | CDK1 |
| GW274150 intracellular | NOS2 |
| Setiptiline extracellular region | ADRA2C |
| Priralfinamide intracellular | MAOB |
| Resatorvid extracellular region | TLR4 |
| E5531 extracellular region | TLR4 |
| AZD8055 intracellular | MTOR |
| XEN-D0101 extracellular region | KCNA5 |
| Deriglidole extracellular region | ADRA2C |
| Dalfampridine extracellular region | KCNA5 |
| Ketamine extracellular region | GRIN3A |
| Gemfibrozil intracellular | LPL |
| Efaroxan extracellular region | ADRA2C |
| Idazoxan extracellular region | ADRA2C |
| Vernakalant extracellular region | KCNA5 |
| Temsirolimus intracellular | MTOR |
| Memantine extracellular region | GRIN3A |
| Everolimus intracellular | MTOR |
| Sorafenib intracellular | RAF1 |
| Azepexole extracellular region | ADRA2C |
| Fipamezole extracellular region | ADRA2C |
| Naphazoline extracellular region | ADRA2C |
| SL251188 intracellular | MAOB |
| Lusaperidone extracellular region | ADRA2C |
| Sirolimus intracellular | MTOR |
| Brimonidine extracellular region | ADRA2C |
| Piperoxan extracellular region | ADRA2C |
| OPC28326 extracellular region | ADRA2C |
| Besipirdine extracellular region | ADRA2C |
| Guanethidine extracellular region | ADRA2C |
| Mianserin extracellular region | ADRA2C |
| Dipivefrine extracellular region | ADRA2C |
| Roniciclib intracellular | CDK1 |
| Suramin extracellular region | PDGFB |
| Yohimbine extracellular region | ADRA2C |
| Ibrolipim extracellular region | LPL |
| Rasagiline intracellular | MAOB |
| Tramazoline extracellular region | ADRA2C |
| AT7519M intracellular | CDK1 |
| Apraclonidine extracellular region | ADRA2C |
| R547 intracellular | CDK1 |
| Alvocidib intracellular | CDK1 |
| (R)-Selegiline intracellular | MAOB |
| Nialamide intracellular | MAOB |

**Figure S12**: Drugs targeting hNPC DE genes. Using Metacore's drug mapping tool, DE genes corresponding to stress relaxation, stiffness, and ligand density were aggregated and interrogated, yielding these 48 drugs that target genes in that list.

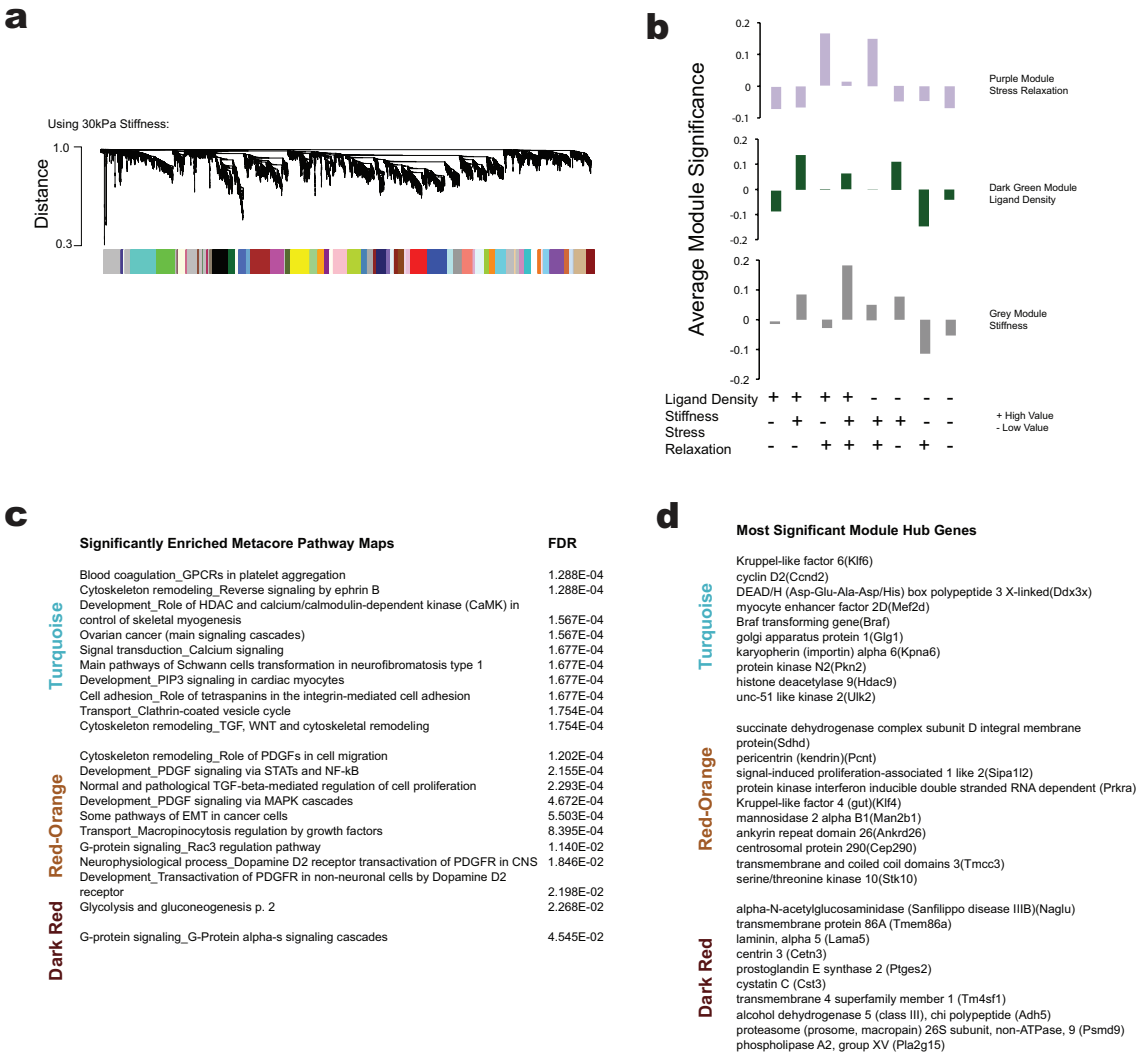


**Figure S13:** Supplementary WGCNA analysis for mMSCs.

a) Cluster dendrogram of gene expression showing module identification from WGCNA analysis using an unsigned network and a soft thresholding parameter of 10 for the dataset containing 30kPa hydrogels as the stiffest condition.

b) Selection of modules that most closely map to ligand density, stiffness, and stress relaxation for the dataset containing 30kPa hydrogels as the stiffest condition. Average module significance is plotted as a function of each material, showing the lack of correspondence between the module and that parameter of interest.

c) Significantly enriched Metacore Pathway Maps from Figure 3 that uses 18kPa as the stiff condition in the WGNCA analysis. The enrichment analysis was carried

435 out using the genes for each module. The turquoise, red-orange, and dark red
436 modules correspond to ligand density, stiffness, and stress relaxation,
437 respectively.
438 d) Significantly enriched module hub genes from Figure 3 that uses 18kPa as the
439 stiff condition in the WGNCA analysis as identified using the WGCNA
440 AnalyzeNetwork function. The genes represent those in each module that have the
441 highest module membership and intramodule connectivity scores. The turquoise,
442 red-orange, and dark red modules correspond to ligand density, stiffness, and
443 stress relaxation, respectively.
444
445
446

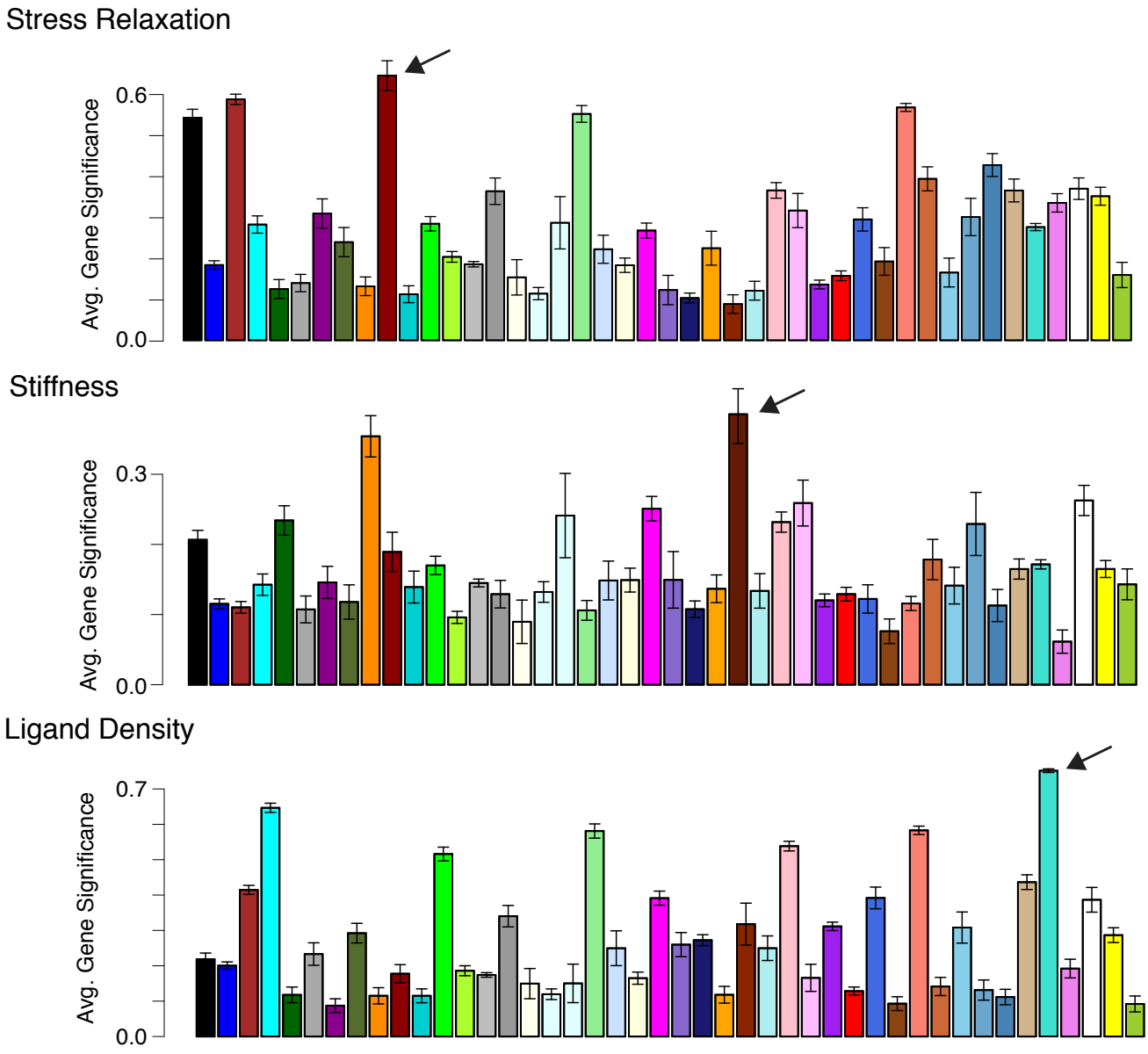


**Figure S14:** Identification of WGCNA modules corresponding to material parameter of interest in mMSCs. Average gene significance for each module with respect to each parameter. The most significant modules were chosen for further analysis and are highlighted with arrows. Mean +/- S.D.

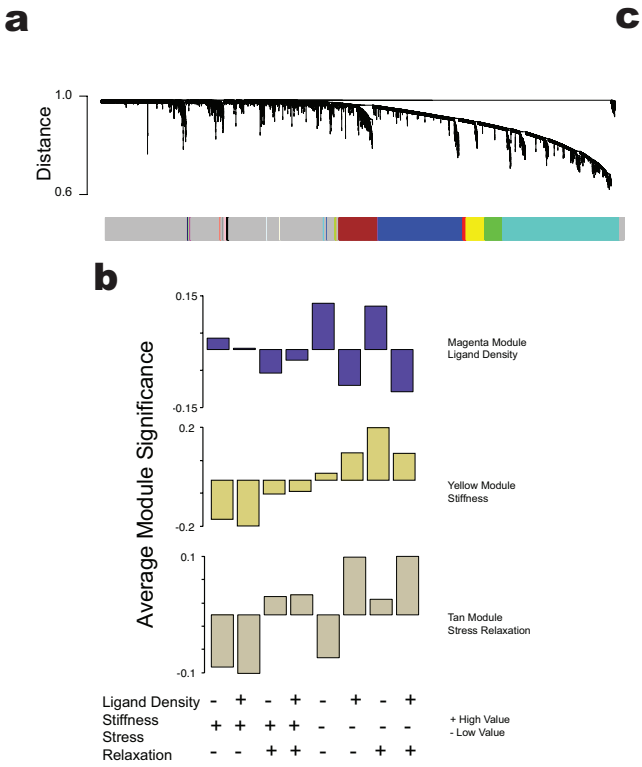


c

| Yellow Module (Stiffness) | log10(FDR) |
|---|---|
| negative regulation of macroautophagy | -3.56676 |
| Endocytosis | -3.08598 |
| axon development | -3.00555 |
| chromatin assembly or disassembly | -2.87697 |
| positive regulation of protein localization to membrane | -2.8579 |
| sensory organ development | -2.8017 |
| Glycosaminoglycan metabolism | -2.73669 |
| Signaling by WNT | -2.56124 |
| mRNA surveillance pathway | -2.17119 |
| negative regulation of kinase activity | -2.16954 |
| endomembrane system organization | -2.15797 |
| **Tan Module (Stress Relaxation)** | |
| extracellular matrix organization | -9.75498 |
| mRNA processing | -7.67582 |
| cell adhesion mediated by integrin | -5.3916 |
| collagen metabolic process | -4.8184 |
| cellular response to growth factor stimulus | -4.57864 |
| Degradation of the extracellular matrix | -4.53725 |
| transmembrane receptor protein tyrosine kinase signaling pathway | -3.68879 |
| DNA conformation change | -3.58599 |
| tissue morphogenesis | -3.40911 |
| blood vessel development | -3.01378 |
| Interleukin-4 and 13 signaling | -2.92789 |
| plasma membrane bounded cell projection morphogenesis | -2.89505 |
| Hippo signaling pathway | -2.36863 |
| cellular response to mechanical stimulus | -2.34469 |
| response to toxic substance | -2.29868 |
| organ growth | -2.19993 |
| regulation of actin filament bundle assembly | -2.18529 |
| Transport to the Golgi and subsequent modification | -2.08234 |
| **Magenta Module (Ligand Density)** | |
| protein localization to membrane | -7.53534 |
| midbrain development | -6.9399 |
| mesenchyme morphogenesis | -4.3201 |
| calcium-independent cell-cell adhesion via plasma membrane cell-adhesion | -3.95918 |
| negative regulation of neuron death | -3.91246 |
| post-translational protein modification | -3.34321 |
| neurotransmitter transport | -3.33242 |
| response to toxic substance | -3.04552 |
| body morphogenesis | -2.97533 |
| positive regulation of cellular protein localization | -2.86132 |
| regulation of potassium ion transmembrane transport | -2.38091 |
| negative regulation of transcription by RNA polymerase II | -2.30819 |
| transmembrane receptor protein tyrosine kinase signaling pathway | -2.08749 |

**Figure S15:** WGCNA analysis of hNPC data. A) Cluster dendrogram identifying colored modules of highly coexpressed genes in the hNPC dataset. B) The correspondence of the three modules showing the highest correlations to our parameters of interest. Each +/- corresponds to the low or high value of each material property and the average normalized expression for each module in each of the eight materials is plotted. C) Metacore PathwayMaps corresponding to the three modules identified in B), along with each term's associated FDR.

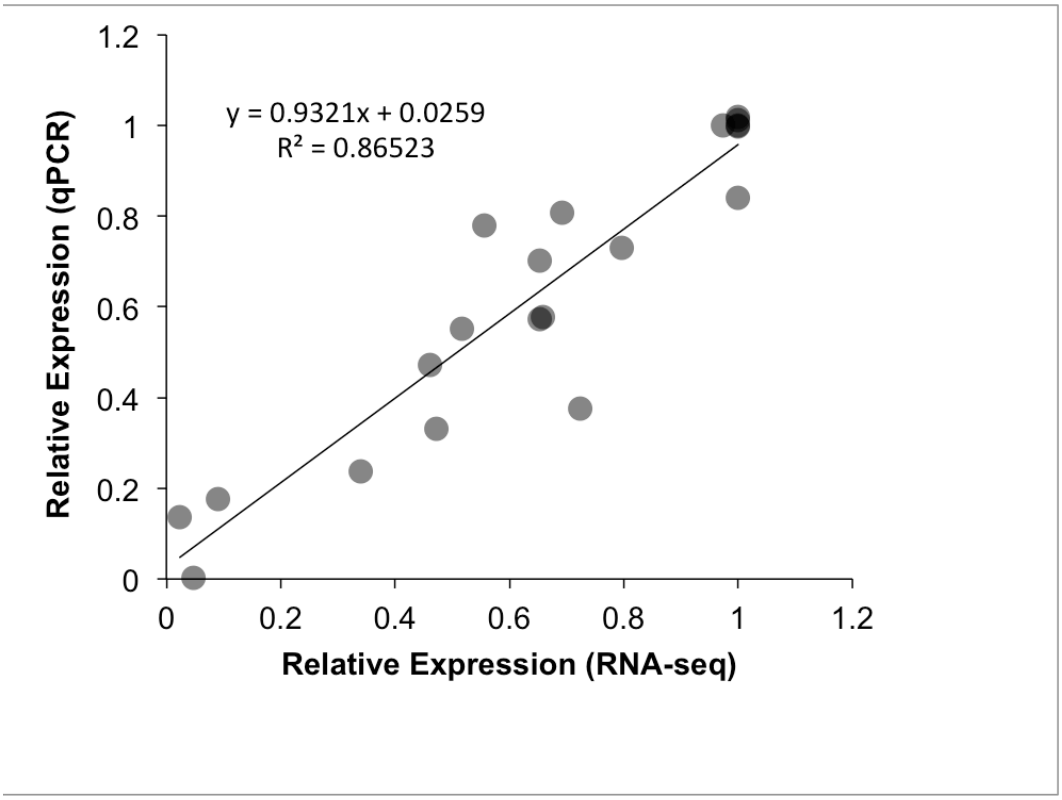


**Fig. S16:** Validation of mMSC RNA-seq results by qPCR. Sampled DE genes for qPCR analysis were Ptges2, E2F7, Bmp3, Zyx, Klf6. This validation experiment was carried out in slow-relaxing 3kPa LLD, slow-relaxing 18kPa LLD, slow-relaxing 3kPa HLD, and slow-relaxing 18kPa HLD hydrogels. Each data point represents a specific transcript for a specific material.

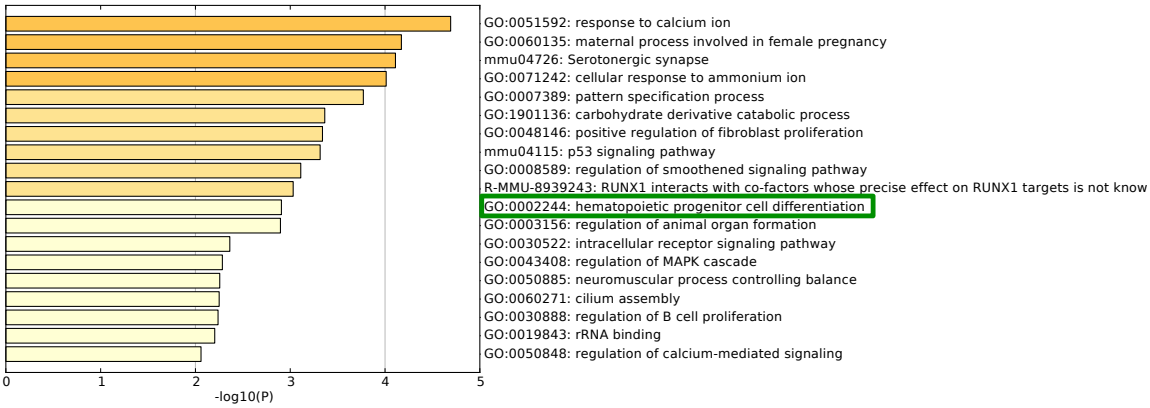


**Figure S17: Gene Ontology results from the top stiffness-related mMSC WGCNA module.** The top 100 most enriched genes in the red-orange module were used as inputs for a gene ontology analysis using Metascape. The plot depicts p-values for each term as determined by Metascape.

| Cyokines Common to RNAseq and Array | Cyokines DE in RNAseq data | Cyokines with Matching Highest Conditions (5/6) |
|---|---|---|
| Mmp2 | Mmp2 | Mmp2 |
| Ccl5 | Opn | Opn |
| Opn | Tnfrsf1b | Tnfrsf1a |
| Tnfrsf1b | Tnfrsf1a | Mcp1 |
| Tnfrsf1a | Mcp1 | Cxcl12 |
| Cx3cl1 | Cxcl12 | |
| Vcam1 | | **Cyokines with Mismatched Highest Conditions (1/6)** |
| Mcp1 | | Tnfrsf1b |
| Ccl17 | | |
| Il13 | | |
| Lix1l | | |
| Il4 | | |
| Selp | | |
| Cxcl12 | | |
| Lepr | | |

**Figure S18:** Correspondence between cytokine array and RNAseq data. Of the cytokines common to both RNAseq and the cytokine array, those showing differential expression in RNAseq were selected. Since there is a mismatch in sensitivity and granularity between the array and RNAseq that prevents direct comparison, the material conditions that corresponded to the highest expression of each cytokine were found and compared.

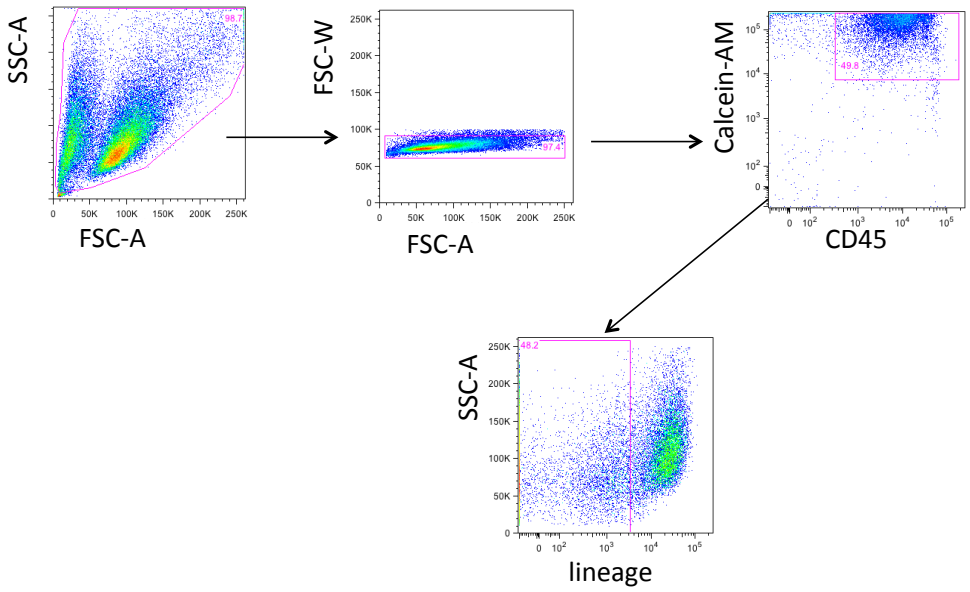


**Figure S19:** Example gating strategy for CD45+/lin- cells.

**Supplemental Tables**

| Supplier | Unique Assay ID | Gene |
|---|---|---|
| BioRad | qMmuCID0005139 | Ptges2 |
| BioRad | qMmuCID0018612 | Gapdh |
| BioRad | qMmuCID0008584 | Bmp3 |
| BioRad | qMmuCID0010274 | E2F7 |
| BioRad | qMmuCID0006114 | Zyx |
| BioRad | qMmuCID0016866 | Klf6 |

**Table S1**: PCR primers used for RNAseq validation

## References


1. Alsberg E, Anderson KW, Albeiruti A, Franceschi RT, & Mooney DJ (2001) Cell-interactive Alginate Hydrogels for Bone Tissue Engineering. *Journal of Dental Research* 80(11):2025-2029.
2. Chaudhuri O*, et al.* (2016) Hydrogels with tunable stress relaxation regulate stem cell fate and activity. *Nat Mater* 15(3):326-334.
3. Huebsch N*, et al.* (2010) Harnessing traction-mediated manipulation of the cell/matrix interface to control stem-cell fate. *Nat Mater* 9(6):518-526.
4. Johnson TD*, et al.* (2016) Quantification of decellularized human myocardial matrix: A comparison of six patients. *PROTEOMICS – Clinical Applications* 10(1):75-83.
5. Taroni P*, et al.* (2015) Breast Tissue Composition and Its Dependence on Demographic Risk Factors for Breast Cancer: Non-Invasive Assessment by Time Domain Diffuse Optical Spectroscopy. *PLoS ONE* 10(6):e0128941.
6. Fischbach C*, et al.* (2009) Cancer cell angiogenic capability is regulated by 3D culture and integrin engagement. *Proceedings of the National Academy of Sciences* 106(2):399-404.
7. Legant WR*, et al.* (2010) Measurement of mechanical tractions exerted by cells within three-dimensional matrices. *Nature methods* 7(12):969-971.
8. Wessendorf AM & Newman DJ (2012) Dynamic Understanding of Human-Skin Movement and Strain-Field Analysis. *IEEE Transactions on Biomedical Engineering* 59(12):3432-3438.
9. Gordon AM, Huxley AF, & Julian FJ (1966) The variation in isometric tension with sarcomere length in vertebrate muscle fibres. *The Journal of Physiology* 184(1):170-192.
10. Huh D*, et al.* (2010) Reconstituting Organ-Level Lung Functions on a Chip. *Science* 328(5986):1662.
11. Liao Y, Smyth GK, & Shi W (2013) The Subread aligner: fast, accurate and scalable read mapping by seed-and-vote. *Nucleic Acids Research* 41(10):e108.
12. Liao Y, Smyth GK, & Shi W (2013) featureCounts: an efficient general-purpose read summarization program. *Bioinformatics*).
13. Law CW, Chen Y, Shi W, & Smyth GK (2014) voom: precision weights unlock linear model analysis tools for RNA-seq read counts. *Genome Biology* 15(2):1-17.
14. Ritchie ME*, et al.* (2015) limma powers differential expression analyses for RNA-sequencing and microarray studies. *Nucleic Acids Research* 43(7):e47.
15. Zhang B & Horvath S (2005) A General Framework for Weighted Gene Co-expression Network Analysis. *Stat Appl Genet Mol Biol* 4.